Defect rich copper oxide nanosheets for selective electrochemical conversion of CO_2 to multi-carbon products at high current density

Weibo Hu
Shanghai Advanced Research Institute, Chinese Academy of Sciences
Lushan Ma
Nanjing University of Science and Technology
Yanping Zhu
Shanghai Advanced Research Institute, Chinese Academy of Sciences
Jiejie Li
ShanghaiTech University
Wenhao Li
Shanghai Advanced Research Institute, Chinese Academy of Sciences
Xingming Ni
ShanghaiTech University
Liangliang Zou
Shanghai Advanced Research Institute, Chinese Academy of Sciences
Zhiqing Zou
Shanghai Advanced Research Institute, Chinese Academy of Sciences
Bo Yang
ShanghaiTech University https://orcid.org/0000-0001-6904-6646
Fan Yang
ShanghaiTech University https://orcid.org/0000-0002-1406-9717
Ke Wen
Shanghai Advanced Research Institute, Chinese Academy of Sciences
Hui Yang (yangh@sari.ac.cn)
Shanghai Advanced Research Institute, Chinese Academy of Sciences

Article

Keywords: CO2 reduction, multi-carbon products, copper oxide nanosheets (CuO-st)

Posted Date: October 22nd, 2021

DOI: https://doi.org/10.21203/rs.3.rs-989906/v1

Abstract

Highly selective electrochemical reduction of CO_2 (CO_2RR) to multi-carbon (C_{2+}) products at high current density remains a big challenge. Herein we report copper oxide nanosheets (CuO-st) for selective electrochemical conversion of CO_2 to C_{2+} products at high current density. Benefiting from the defect-rich structure verified by HR-TEM and XPS characterization and the designed gas diffusion electrode, such a CuO-st material exhibits CO_2RR FE (C_{2+}) of 86 and 80 % at 1.0 and 1.8 A cm^{-2}, respectively, with excellent durability of 50 h @ 500mAcm^{-2} and storable lifetime for >10 months. Importantly, using quasi-situ XPS and in-situ Roman spectra, we have shown the first evidence for the presence of Cu (δ) during the eCO_2RR on initial Cu (δ) material, and the proportion of Cu (δ) varies with the reaction current density. The rough and defective surface of CuO-st serves as a favorable reservoir to produce enough Cu (δ) to assist the C-C coupling, thus achieving selective CO_2RR to C_{2+} products at high current density. Our study not only provides a new insight into CO_2RR, but also suggests that in-situ forming active species from stable Cu (δ) materials during the reaction may be a good choice for the practical application, which will be very helpful to the development of cost-effective CO_2RR electrocatalysts.

Introduction

The transformation of CO_2 into value-added products using renewable power offers a promising strategy to solve the energy and environment crisis, and therefore has drawn increasing interest in academic and industry.[1–6] Various carbon-based chemicals can be obtained through the electrochemical CO_2 reduction reaction (eCO_2RR), among which, the deeply reduced ones, such as multi-carbon (C_{2+}) molecules, are preferred. Copper (Cu) based catalysts are known as the only family which can produce considerable amounts of C_{2+} products in eCO_2RR.[7–9] However, it is difficult to achieve high C_{2+} selectivity because the formation of such products involves an eight or more electron transfer process, while the less-electron transfer involved products, such as CO and CHOOH, are easier to form.[10,11]

The C–C coupling of eCO_2RR intermediates (CO*, CHO* and et.al) results in producing C_{2+} molecules or else to C1 products.[10–16] Oxide-derived Cu materials have been reported to have good selectivity for C_{2+} products. Surface residual O on Cu has been suggested to stabilize CO*, promoting C–C coupling.[17–20] However, in some oxide-derived Cu involved systems, O is found to disappear in eCO_2RR.[21–22] In addition to O, residual Cu (δ) has also been revealed to assist the C–C coupling possess.[23–27] Up to now, Cu_2O modified Cu catalysts are the main oxide-derived Cu material type which have been extensively studied in eCO_2RR. Besides oxide-derived Cu, Cu materials with abundant high-index facets or defects, also have showed good selectivity for C_{2+} products.[28–35]

Although valuable progresses have been made, numerous challenges are still existing. Firstly, some reported catalysts have showed excellent Faraday efficiency (FE) for multi-carbon (C_{2+}) products (> 80%), but selectively converting CO_2 at high current densities (> 1 A cm^{-2}) remains as a challenge. Secondly,

some oxide-derived Cu materials have showed good C_{2+} selectivity, but the role of O or Cu (δ) is still on debate. Thirdly, most of the reported efficient catalysts need complicated preparation process with limited synthetic quantity, and it is still difficult to scale up the production. Additionally, sub-nano structured Cu or Cu/Cu_2O, especially those with high-index facets are easy to degenerate in air, which makes the materials hard to store and sale as commodities. In this aspect, in-situ forming active Cu species in the course of eCO_2RR from stable precursors could be a good choice.

Herein, we developed a wet chemistry method for the preparation of copper oxide nanosheets (CuO-st). Field emission scanning electron microscopy (FE-SEM), transmission electron microscopy (TEM) and X-ray photoelectron spectroscopy (XPS) revealed that CuO-st possessed a rough and defective surface. CuO-st showed excellent C_{2+} selectivity (mainly C_2H_4, ethanol and propanol) at high current density, with FE (C_{2+}) of 86 and 80 % at 1.0 and 1.8 A cm^{-2}, respectively. Outstandingly, excellent catalytic stability was also achieved (@ ~580 mA cm^{-2}, 50 h). The C–C coupling rate was found positively correlated with the concentration of KCl once the reaction initiated in flow cell. Mechanistic study indicated the existence of Cu (δ) in the CuO-st derived copper species during eCO_2RR, and the amount of Cu (δ) varied with the reaction. Moreover, CuO-st showed good storage stability, without distinctive changes in powder X-ray diffraction (PXRD) and eCO_2RR performance after more than 10 months exposed to air.

Synthesis and characterization of the catalysts. Copper oxide (CuO-st) was synthesized in gram scale with hydrazine hydrate as an initiator (see the Methods for details). By adjusting the reaction condition, cuprous oxide (Cu_2O-pt) and copper (Cu-pt) were prepared for comparison. The composition of the materials were firstly confirmed by powder X-ray diffraction (PXRD) (Supplementary Fig. 1-3). The morphologies were investigated using field emission scanning electron microscopy (FE-SEM). Cu_2O-pt was revealed to have octahedron structures (Supplementary Fig. 6), while Cu-pt was amorphous particles (Supplementary Fig. 7). CuO-st possessed a sheet-like structure under low magnification (Fig. 1a), but the high power SEM images revealed that the nanosheets had rough surface, forming by the accumulation of nano-particulates with an average diameter of 20 ± 3 nm (Fig. 1b). CuO-st was further studied by transmission electron microscopy (TEM). The low-resolution image showed a sheet-like structure (Fig. 1c and d). The HR-TEM image exhibited that the spacing of the lattice planes were ~0.27 and 0.23 nm, which corresponded well to (110) and (111) planes of copper oxide, respectively (Fig. 1e). Interestingly, lattice dislocation could be observed in the HR-TEM images (Fig. 1e and Supplementary Fig. 5), indicating the existence of rich defects. Such a nature was further confirmed by X-ray photoelectron spectroscopy (XPS) analysis. As shown in Fig. 1f, the O 1s region of CuO-st can be fitted into three peaks with binding energy (BE) of 592.6, 531.3 and 533.0 eV, respectively. The peak at 592.6 eV was attributed to lattice oxygen, the minor peak at 533.0 eV was assigned to the surface hydroxide or chemisorbed oxygen, and the peak between them (531.3 eV) was attributed to defective oxygen.[36–38] The radio of defective oxygen/ lattice oxygen is close to 1/2.1 (Supplementary Table 1).

Electrochemical performance evaluation. The eCO_2RR performance of the catalysts were firstly studied with an H-cell. We analyzed the gas and liquid products at the applied potentials between −0.85 and

−1.40 V (vs RHE) in CO_2-saturated 0.1 M KCl (pH 3.8). It could be observed that the C-C coupling efficiency improved steadily once the voltage decreased from -0.9 to -1.2 V (vs RHE) for all the materials. For CuO-st, the FEs of C_2H_4 and C_{2+} products reached up to 58 and 82 % at −1.21 V (vs RHE), respectively, while the formation of CH_4 and H_2 remained at very low levels at all the tested potential range. Cu-pt and Cu_2O-pt showed maximum FE (C_{2+})s of 73 and 68 % at -1.24 and - 1.28 V (vs RHE), respectively, lower than the one of CuO-st. Additionally, the partial current of C_{2+} products (j(C_{2+})) of CuO-st was the highest among the three materials achieved (Supplementary Fig. 8-10). The results indicate that CuO-st has better performance than Cu-pt and Cu_2O-pt in selective conversion of CO_2 to C_{2+} products.

To explore the possible use of CuO-st in industry, we further evaluated the eCO_2RR selectivity in a flow cell. The FEs distribution of cathode products vs currents in 1 M KCl, 2M KCl and saturated KCl (sa. KCl) are shown in Fig. 3a-c. It was revealed that the FE (C_{2+}) showed an increase in all the solutions when the constant current density was raised from 600 mA cm^{-2} to 1.0 A cm^{-2}. The FE (C_{2+}) seemed to have a positive correlation with the KCl concentration. In sa. KCl, the FE (C_{2+}) at 1.0 and 1.8 A cm^{-2} were achieved 86 and 80 %, respectively. Such an excellent C_{2+} selectivity at high reaction rate almost represents the state-of-the-art performance of Cu-based catalysts. (Fig. 3f and Supplementary Table 2). Potentiostatic electrolysis was chose for the stability test. It was observed that during the operation of the reaction at -0.98 V (vs RHE, with iR correction) in 1 M KCl for ~50 h, the current density kept ~580 mA cm^{-2} and the FE (C_2H_4) showed no significant change (Supplementary Fig. 17). Moreover, storability of CuO-st was also evaluated. It was revealed that no distinctive change happened in the PXRD and eCO_2RR performance of CuO-st after in air for ~10 months (Supplementary Fig. 18 and 19).

Mechanism And Discussion

The eCO_2RR happens at the potentials negative to the CuO reduction reaction, so reconstruction may take place during the eCO_2RR process. We observed that after the eCO_2RR, the color of the electrode changed from grey to red, and then to yellow in 1h. XRD was used to disclose such phenomenon. As shown in Supplementary Fig. 22, the used CuO-st electrode shows no signals of CuO any longer, but the pattern of Cu (0), while the yellow electrode shows the ones of Cu_2O. We speculated that CuO-st was almost reduced to Cu (0) species during eCO_2RR, which would be re-oxidized in air easily. In situ x-ray absorption spectroscopy (XAS) study provided more evidence. The XAS of CuO-st showed the spectra matching with CuO at first. When a potential of -1.2 V (vs RHE) applied for 20 mins, the observed spectra became close to the ones of Cu foil (Supplementary Fig. 23).

To investigate the surface structure of CuO-st during eCO_2RR and the origin of the excellent C_{2+} selectivity, in-situ Raman spectroscopy measurements were performed. As shown in Supplementary Fig. 24, at open circuit potential (OCP), two peaks at 1339 and 1619 cm^{-1} are observed, which may be caused by the adsorption of CO_2 on the rough and defective surface of CuO-st. At a current density of 40 mA cm^{-2}, peaks at around 275, 360, 527 and 1064 cm^{-1} became obvious (Fig. 4a). With increasing the

current, the peaks at 275 and 1064 cm^{-1} disappeared, and the ones at around 360 and 527 cm^{-1} weakened. This might be resulted by the signal inhibition effect of the bubbles formed during the reaction or the potential-dependent reaction-path change. Once the voltage was removed, several new peaks appeared, but became weaker over time (Fig. 4a and c). Those peaks could be assigned to the adsorbed intermediates formed during eCO_2RR, including the bicarbonate at 1031 cm^{-1}, hydrogenated species at 813, 1227, 1265, 1390, 1574 and 2907 cm^{-1},[39] and *CO at 1930 cm^{-1}. It should be mentioned that those intermediates are common species for C_{2+} products formation. After the applied potential returned to OCP, the peak at 275 cm^{-1} became significant again (Fig. 4c). At such a stage, the eCO_2RR intermediates have almost gone. Compared with the previous report, it is reasonable to ascribe the peak at around 275 cm^{-1} to the adsorbed Cl* (Cu-Cl*).[40] The vibrations of Cu-C [41–44] and Cu_xO/-OH*[45,46] may appear at 520-550 cm^{-1}. As the signal around 527 cm^{-1} showed an obvious decrease but still existed when the voltage was removed (Fig. 4a-c), we speculated that such a peak was mainly consisted by the reaction intermediate (Cu-C), and accompanied by certain amount of Cu_xO/-OH* as the residual after returning to OCP. Fig. 4b shows the partial spectra of Fig. 4a in the box. It could be observed that the peak of Cu-C vibration was visibly shifted to higher place with the increasing of the reaction rate, and returned to lower frequency once the reaction stopped (Fig. 4b). Previous reports have demonstrated that increasing the proportion of charged metal (M) could strengthen the M-adsorbate interaction, inducing blue shifts.[47] However, Stark effect which also can cause such changes is hard to be rule out here. Quasi-in situ XPS was used to further disclose the structural change of the catalyst. After the reactions, the BEs of Cu 2p of CuO-st (CuO-st-40, CuO-st-1000 and CuO-st-1400) all shifted to ~ 932.5 eV (Supplementary Fig. 25), and the main Cu LMM peaks were close to 918.4 eV (Fig. 4d), indicating that CuO-st was almost reduced to Cu (0). However, the Cu LMM spectra also showed the signal of Cu (□) species (Fig. 4d).[48] The spectra of O 1s and Cl 2p regions provide more information. The O 1s of the CuO-st-40 showed a peak at ~530 eV, which matched with the BE of lattice O in Cu_2O. As such a peak disappeared in CuO-st-1000 and CuO-st-1400 (Fig. 4e), we speculated the Cu_2O in CuO-st-40 formed because of the partial reduction of CuO-st. Fig. 4f shows the Cl 2p regions. Interestingly, it could be observed that the BEs persisted a positive relationship with the reaction (C-C coupling) rate, and being much closer to the BE of Cu-Cl after the reaction at a current density of 1400 mA/cm^2. Such a phenomenon should be caused by the difference in the amount of Cu (□) on CuO-st derived Cu species surface. More Cu (□) exists during the reaction, and more Cu-Cl bonds will form after the reaction. The results here provide the first evidence for the presence of Cu (□) during the Cu (□) material catalyzed eCO_2RR, and indicate that the proportion of Cu (□) would vary with the reaction. The rough and defective surface of CuO-st serves as a favorable reservoir to produce enough Cu (□) to assist the C-C coupling, achieving selective conversion of CO_2 to C_{2+} products at high current density.

As the FE (C_{2+}) showed a positive correlation with the KCl concentration in flow cell (Fig. 3), we studied the electrolyte effect on CuO-st. The linear sweep voltammetry (LSV) tests were conducted in different concentration of KCl solutions. It turned out that the curves shifted markedly with the increase of the concentrations (Fig. 5a) under CO_2 atmosphere, while remained relatively constant under Ar

(Supplementary Fig. 26), indicating the close HER activity but varied eCO_2RR performance. The Tafel plots of C_2H_4 in 0.5 M and 2 M KCl solutions were calculated. As shown in Fig. 5b, the plots present good linearity with a slope of 78.2 mV dec^{-1} in 2 M KCl, smaller than the one in 0.5 M KCl (97.9 mV dec^{-1}). The results demonstrate that in these two solutions a same rate-determining step exists. The gas products of the eCO_2RR in 0.5 M KCl and 2 M KCl were analyzed at different applied potentials (after iR corrections). The highest FE (C_2H_4) in these two solution only showed ~5 % apart, but the over-potentials to achieve the FE differed greatly (~1 V, Fig. 5c and d). The J (C_2H_4) and J (C_2H_4) / J (CO) in 2 M KCl were 100 and 14-times, respectively, higher than those in 0.5 M KCl at -1.0 V (vs RHE, Supplementary Fig. 27). The results indicate that the eCO_2RR, especially C–C coupling, is getting faster with the increase of the KCl concentration once the reaction initiated.

Both cations and anions have been reported to affect the eCO_2RR selectivity, but the effect varies with the catalysts and systems.[49–54] Lee and his coworkers reported that Cl^- could assist the C–C coupling,[49] while Strasser and his coworkers showed that Cl^- increased CO selectivity.[50] Cationic species have been demonstrated to affect C_{2+} reaction pathways through the electrostatic interactions.[51–54] In order to further illustrate the effect of the electrolyte, the eCO_2RR performance of CuO-st in different electrolytes were evaluated. It was revealed that the FE (C_2H_4) in KCl (2 M) was very close to the ones in KI (2 M), KOH (2 M) and KBr (2 M) at the current density of 1 A cm^{-2} (Supplementary Fig. 28), indicating that the effect of the studied anions on the C_{2+} selectivity was not significant.[51] The cation effect seemed to be much more pronounced (Supplementary Fig. 29). In 1 M NH_4Cl, the FE (C_2H_4) decreased to 1.3% at the current density of 600 mA cm^{-2}, while the FE (H_2) increased to 73%. We speculated that the moderated anion effect might be caused by the OH^- produced during eCO_2RR. Supposing that the protons of the eCO_2RR products are all from H_2O, the local concentration of OH^- proximity to the catalyst surface is possibly higher than the anion from bulk electrolyte when the eCO_2RR are performed at high reaction rate.[55–58] Indeed, the quasi-situ XPS spectra of the samples electrolyzed at high current density showed pronounced peaks at ~532.8 eV (Fig. 5e), closing to the BE of reported OH.[37] Therefore, K^+ may be the major contributor to the electrolyte-concentration-related C-C coupling efficiency change in this study.

Conclusions

In summary, we have developed the scalable synthetic method for the preparation of copper oxide nanosheets (CuO-st) with rich defects, and demonstrated for the first time that Cu (□) exists during the eCO_2RR on initial Cu (□) material, and the proportion of Cu (□) varies with the reaction current density, as evidenced by quasi-situ XPS and in-situ Roman spectra. The rough and defective structure of CuO-st serves as a reservoir to produce enough Cu (□) to achieve the current over 1 A cm^{-2} with a FE (C_{2+}) above 80%, exceeding the CO_2RR performance of the previously reported Cu-based catalysts. Our study indicates that in-situ producing active Cu species from stable Cu (□) materials in the eCO_2RR process is a good choice for the practical application. The initial valence of Cu within a material may possess no

controlling role on the C_{2+} formation, while lattice defects and morphology properties of the catalysts, together with electrolyte, support the high selectivity of CO_2RR.

Methods

In situ X-ray absorption spectroscopy. XAS measurements were carried out at the BL14W1 beamline in Shanghai Synchrotron Radiation Facility (SSRF). The data were collected using a fixed-exit double-crystal Si (111) monochromator. The hydrophobic carbon paper was used as the substrate for supporting CuO-st to prepare the working electrode for the tests. A custom-designed in-situ cell coupled with the three-electrode system was utilized. During the operando measurements, CO_2 was continuously bubbled into the electrolyte (0.1 M KCl). Lytle detector was used to collect the fluorescence signal of the Cu K-edge (8979 eV) XAFS spectra.

In-situ Raman. The Raman was recorded on a HORIBA LABRAM HR Evolution Raman spectrometer. In the measurements, the GDE was similar to the ones in electrochemical measurements, and CO_2 was continuously injected into the gas chamber, with saturated KCl as the cathode electrolyte, saturated K_2SO_4/0.05 M H_2SO_4 as the anode electrolyte, and nafion 115 as the separator. Each current was applied for around 5 min before collecting the spectra.

Quasi-in situ XPS. The XPS was performed on ESCALAB 250XI X-ray photoelectron spectrometer with an Al Kα radiator and the vacuum in the analysis chamber was maintained at approximately 10^{-10} mbar. The binding energy was calibrated by the C 1s peak energy at 284.8 eV. The GDEs were similar to the ones in electrochemical measurements and the reactions were performed in the glovebox for 30 mins, with saturated KCl as the cathode electrolyte, saturated K_2SO_4/0.05 M H_2SO_4 as the anode electrolyte, and nafion 115 as the separator. After the reactions, the electrodes were washed with deionized water in glovebox, and transferred by the X-ray photoelectron spectroscopy portable device to realize the quasi-in-situ tests. During the test, the produced O_2 were expelled out of glovebox, and the concentration of O_2 in glovebox kept under 0.01ppm.

Declarations

Acknowledgements

This work was financially supported by the National Key Research and Development Programs of China (2017YFA0206500, 2017YFB0602205), the National Natural Science Foundation of China (21902176, 21872165, 21991152, 21991150, 52106248, 21972144, 91845109), the DNL Cooperation Fund, CAS (DNL201924), Shanghai Sailing Program (19YF1452900), Youth Innovation Promotion Association CAS (2020291), and the Basic Science Center Program for Ordered Energy Conversion of the National Natural Science Foundation of China (51888103). We also greatly thank for the beam time provided by the BL14W1 beamline of Shanghai Synchrotron Radiation Facility (SSRF).

Author contributions

Weibo Hu, Ke Wen and Hui Yang initiated and supervised the research. Weibo Hu designed the catalysts and carried out the electrochemical experiments. Yanping Zhu, Liangliang Zou and Zhiqing Zou assisted with electrochemical experiments. Wenhao Li recorded the NMR data, Lushan Ma performed the in situ Raman measurements. Xingming Ni and Fan Yang performed the quasi-in situ XPS measurements. Weibo Hu, Hui Yang, Jiejie Li, Bo Yang, Fan Yang contributed to data analysis. Weibo Hu, Ke Wen and Hui Yang wrote the draft.

Competing interests

The authors declare no competing interests.

References

1. Aran-Ais, R. M., Gao, D. & Roldan Cuenya, B. Structure- and electrolyte-sensitivity in CO_2 electroreduction. *Acc. Chem. Res.* **51**, 2906–2917 (2018).
2. Chen, C., Khosrowabadi Kotyk, J. F. & Sheehan, S. W. Progress toward commercial application of electrochemical carbon dioxide reduction. *Chem* **4**, 2571–2586 (2018).
3. Kondratenko, E. V., Mul, G., Baltrusaitis, J., Larrazábal, G. O. & Pérez-Ramírez, J. Status and perspectives of CO_2 conversion into fuels and chemicals by catalytic, photocatalytic and electrocatalytic processes. *Energy Environ. Sci.* **6**, 3112 (2013).
4. Qiao, J., Liu, Y., Hong, F. & Zhang, J. A review of catalysts for the electroreduction of carbon dioxide to produce low-carbon fuels. *Chem. Soc. Rev.* **43**, 631–675 (2014).
5. Sun, Z., Ma, T., Tao, H., Fan, Q. & Han, B. Fundamentals and challenges of electrochemical CO_2 reduction using two-dimensional materials. *Chem* **3**, 560–587 (2017).
6. Zhang, L., Zhao, Z. J. & Gong, J. Nanostructured materials for heterogeneous electrocatalytic CO_2 reduction and their related reaction mechanisms. *Angew. Chem. Int. Ed.* **56**, 11326–11353 (2017).
7. Bagger, A., Ju, W., Varela, A. S., Strasser, P. & Rossmeisl, J. Electrochemical CO_2 reduction: a classification problem. *Chemphyschem* **18**, 3266–3273 (2017).
8. Nitopi, S. *et al.* Progress and perspectives of electrochemical CO_2 reduction on copper in aqueous electrolyte. *Chem. Rev.* **119**, 7610–7672 (2019).
9. Tayyebi, E., Hussain, J., Abghoui, Y. & Skúlason, E. Trends of electrochemical CO_2 reduction reaction on transition metal oxide catalysts. *J. Phys. Chem. C* **122**, 10078–10087(2018).
10. Gao, D., Arán-Ais, R. M., Jeon, H. S. & Roldan Cuenya, B. Rational catalyst and electrolyte design for CO_2 electroreduction towards multicarbon products. *Nat. Catal.* **2**, 198–210 (2019).
11. Fan, L. *et al.* Strategies in catalysts and electrolyzer design for electrochemical CO_2 reduction toward C_{2+} products. *Sci. Adv.* **6**, eaay3111 (2020).

12. Kim, Y. *et al.* Time-resolved observation of C–C coupling intermediates on Cu electrodes for selective electrochemical CO_2 reduction. *Energy Environ. Sci.* **13**, 4301–4311 (2020).
13. Todorova, T. K., Schreiber, M. W. & Fontecave, M. Mechanistic understanding of CO_2 reduction reaction (CO_2RR) toward multicarbon products by heterogeneous copper-based catalysts. *ACS Catal.* **10**, 1754–1768 (2019).
14. Wei, X. *et al.* Highly selective reduction of CO_2 to C_{2+} hydrocarbons at copper/polyaniline interfaces. *ACS Catal.* **10**, 4103–4111 (2020).
15. Zhi, X., Jiao, Y., Zheng, Y. & Qiao, S.-Z. Key to C2 production: selective C–C coupling for electrochemical CO_2 reduction on copper alloy surfaces. *Chem. Commun.* doi: 10.1039/d1cc03796j (2021).
16. Ma, L. *et al.* Covalent triazine framework confined copper catalysts for selective electrochemical CO_2 reduction: operando diagnosis of active sites. *ACS Catal.* **10**, 4534–4542 (2020).
17. Cavalca, F. *et al.* Nature and distribution of stable subsurface oxygen in copper electrodes during electrochemical CO_2 reduction. *J. Phys. Chem. C* **121**, 25003–25009 (2017).
18. Chen, C. *et al.* The in situ study of surface species and structures of oxide-derived copper catalysts for electrochemical CO_2 reduction. *Chem. Sci.* **12**, 5938–5943 (2021).
19. Lum, Y. & Ager, J. W. Stability of residual oxides in oxide-derived copper catalysts for electrochemical CO_2 reduction investigated with $^{(18)}O$ labeling. *Angew. Chem. Int. Ed.* **57**, 551–554 (2018).
20. Zhang, W. *et al.* Atypical oxygen-bearing copper boosts ethylene selectivity toward electrocatalytic CO_2 reduction. *J. Am. Chem. Soc.* **142**, 11417–11427 (2020).
21. Jeong, H. M. *et al.* Atomic-scale spacing between copper facets for the electrochemical reduction of carbon dioxide. *Adv. Energy Mater.* **10**, 1903423 (2020).
22. Lei, Q. *et al.* Investigating the origin of enhanced C_{2+} selectivity in oxide-/hydroxide-derived copper electrodes during CO_2 electroreduction. *J. Am. Chem. Soc.* **142**, 4213–4222 (2020).
23. Jung, H. *et al.* Electrochemical fragmentation of Cu_2O nanoparticles enhancing selective C-C coupling from CO_2 reduction reaction. *J. Am. Chem. Soc.* **141**, 4624–4633 (2019).
24. Kim, C. *et al.* Cu/Cu_2O Interconnected porous aerogel catalyst for highly productive electrosynthesis of ethanol from CO_2. *Adv. Funct. Mater.* **31**, 2102142 (2021).
25. Mistry, H. *et al.* Highly selective plasma-activated copper catalysts for carbon dioxide reduction to ethylene. *Nat. Commun.* **7**, 12123 (2016).
26. Yang, P. P. *et al.* Protecting copper oxidation state via intermediate confinement for selective CO_2 electroreduction to C_{2+} fuels. *J. Am. Chem. Soc.* **142**, 6400–6408 (2020).
27. Zhou, Y. *et al.* Dopant-induced electron localization drives CO_2 reduction to C_2 hydrocarbons. *Nat. Chem.* **10**, 974–980 (2018).

28. Bagger, A., Ju, W., Varela, A. S., Strasser, P. & Rossmeisl, J. Electrochemical CO_2 reduction: classifying Cu facets. *ACS Catal.* **9**, 7894–7899 (2019).
29. Chang, C.-C. & Ku, M.-S. Role of high-index facet Cu (711) surface in controlling the C2 selectivity for CO_2 reduction reaction—a DFT Study. *J. Phys. Chem. C* **125**, 10919–10925 (2021).
30. Li, Y. *et al.* Large single-crystal Cu foils with high-index facets by strain-engineered anomalous grain growth. *Adv. Mater.* **32**, e2002034 (2020).
31. Philip, M., Woldu, A. R., Akbar, M. B., Louis, H. & Cong, H. A facile synthesis of Cu catalysts with multiple high-index facets for the suppression of competing H_2 evolution during electrocatalytic CO_2 reduction. *Nanoscale* **13**, 3042–3048 (2021).
32. Arán-Ais, R. M., Scholten, F., Kunze, S., Rizo, R. & Roldan Cuenya, B. The role of in situ generated morphological motifs and Cu (i) species in C2+ product selectivity during CO_2 pulsed electroreduction. *Nat. Energy* **5**, 317–325 (2020).
33. Li, Z. *et al.* Planar defect-driven electrocatalysis of CO_2-to-C_2H_4 conversion. *J. Mater. Chem. A*, doi: 10.1039/d1ta02565a (2021).
34. Simon, G. H., Kley, C. S. & Cuenya, B. R. Potential-dependent morphology of copper catalysts during CO_2 electroreduction revealed by in situ atomic force microscopy. *Angew. Chem. Int. Ed.* **60**, 2561–2568 (2021).
35. Zhang, B. *et al.* Highly electrocatalytic ethylene production from CO_2 on nanodefective Cu nanosheets. *J. Am. Chem. Soc.* **142**, 13606–13613 (2020).
36. Biesinger, M. C. Advanced analysis of copper X-ray photoelectron spectra. *Surf. Interface Anal.* **49**, 1325–1334 (2017).
37. Shen, Y., Guo, M., Xia, X. & Shao, G. Role of materials chemistry on the electrical/electronic properties of CuO thin films. *Acta Mater.* **85**, 122–131 (2015).
38. Wang, Z. *et al.* Identifying copper vacancies and their role in the CuO based photocathode for water splitting. *Angew. Chem. Int. Ed.* **58**, 17604–17609 (2019).
39. Batista, E. A. & Temperini, M. L. A. Spectroscopic evidences of the presence of hydrogenated species on the surface of copper during CO_2 electroreduction at low cathodic potentials. *J. Electroanal. Chem.* **629**, 158–163 (2009).
40. Niaura, G. & Malinauskas, A. Surface-enhanced Raman scattering from chloride on copper electrodes. *Chem. Phys. Lett.* **207**, 455–460 (1993).
41. Kedzierzawski, P. & Augustynski, J. A Surface enhanced roman scattering study of the intermediate and poisoning species formed during the electrochemical reduction of CO_2 on copper. *J. Electrochem. Soc.* **144**, 4288–4296 (1997).
42. Moradzaman, M. & Mul, G. In situ raman study of potential-dependent surface adsorbed carbonate, CO, OH, and C species on Cu electrodes during electrochemical reduction of CO_2. *ChemElectroChem* **8**, 1478-1485 (2021).

43. Ren, D., Gao, J., Zakeeruddin, S. M. & Gratzel, M. New insights into the interface of electrochemical flow cells for carbon dioxide reduction to ethylene. *J. Phys. Chem. Lett.* **12**, 7583–7589 (2021).
44. Shan, W. *et al.* In situ surface-enhanced Raman spectroscopic evidence on the origin of selectivity in CO_2 electrocatalytic reduction. *ACS Nano* **14**, 11363–11372 (2020).
45. Niaura, G. Surface-enhanced Raman spectroscopic observation of two kinds of adsorbed OH^- ions at copper electrode. *Electrochim. Acta* **45**, 3507–3519 (2020).
46. Chen, C. *et al.* The in situ study of surface species and structures of oxide-derived copper catalysts for electrochemical CO_2 reduction. *Chem. Sci.* **12**, 5938–5943 (2021).
47. Zhao, L.-B., Huang, R., Bai, M.-X., Wu, D.-Y. & Tian, Z.-Q. Effect of aromatic amine–metal interaction on surface vibrational Raman spectroscopy of adsorbed molecules investigated by density functional theory. *J. Phys. Chem. C* **115**, 4174–4183 (2011).
48. Li, Y. *et al.* Crystal-plane-dependent redox reaction on Cu surfaces. *Nano Res.* **13**, 1677–1685 (2020).
49. Lee, S., Kim, D. & Lee, J. Electrocatalytic production of C_3-C_4 compounds by conversion of CO_2 on a chloride-induced bi-phasic Cu_2O-Cu catalyst. *Angew. Chem. Int. Ed.* **127**, 14914–14918 (2015).
50. Varela, A. S., Ju, W., Reier, T. & Strasser, P. Tuning the catalytic activity and selectivity of Cu for CO_2 electroreduction in the presence of halides. *ACS Catal.* **6**, 2136–2144 (2016).
51. Huang, J. E. *et al.* CO_2 electrolysis to multicarbon products in strong acid. *Science* **372**, 1074–1078 (2021).
52. Resasco, J. *et al.* Promoter effects of alkali metal cations on the electrochemical reduction of carbon dioxide. *J. Am. Chem. Soc.* **139**, 11277–11287 (2017).
53. Ringe, S. *et al.* Understanding cation effects in electrochemical CO_2 reduction. *Energy Environ. Sci.* **12**, 3001–3014 (2019).
54. Liu, H., Liu, J. & Yang, B. Promotional role of a cation intermediate complex in C_2 formation from electrochemical reduction of CO_2 over Cu. *ACS Catalysis* **11**, 12336–12343(2021).
55. Dunwell, M. *et al.* Examination of near-electrode concentration gradients and kinetic impacts on the electrochemical reduction of CO_2 using surface-enhanced infrared spectroscopy. *ACS Catal.* **8**, 3999–4008 (2018).
56. Henckel, D. A. *et al.* Potential dependence of the local pH in a CO_2 reduction electrolyzer. *ACS Catal.* **11**, 255–263 (2020).
57. Lu, X. *et al.* In situ observation of the pH gradient near the gas diffusion electrode of CO_2 reduction in alkaline electrolyte. *J. Am. Chem. Soc.* **142**, 15438–15444 (2020).
58. Yang, K., Kas, R. & Smith, W. A. In situ infrared spectroscopy reveals persistent alkalinity near electrode surfaces during CO_2 electroreduction. *J. Am. Chem. Soc.* **141**, 15891–15900 (2019).

Figures

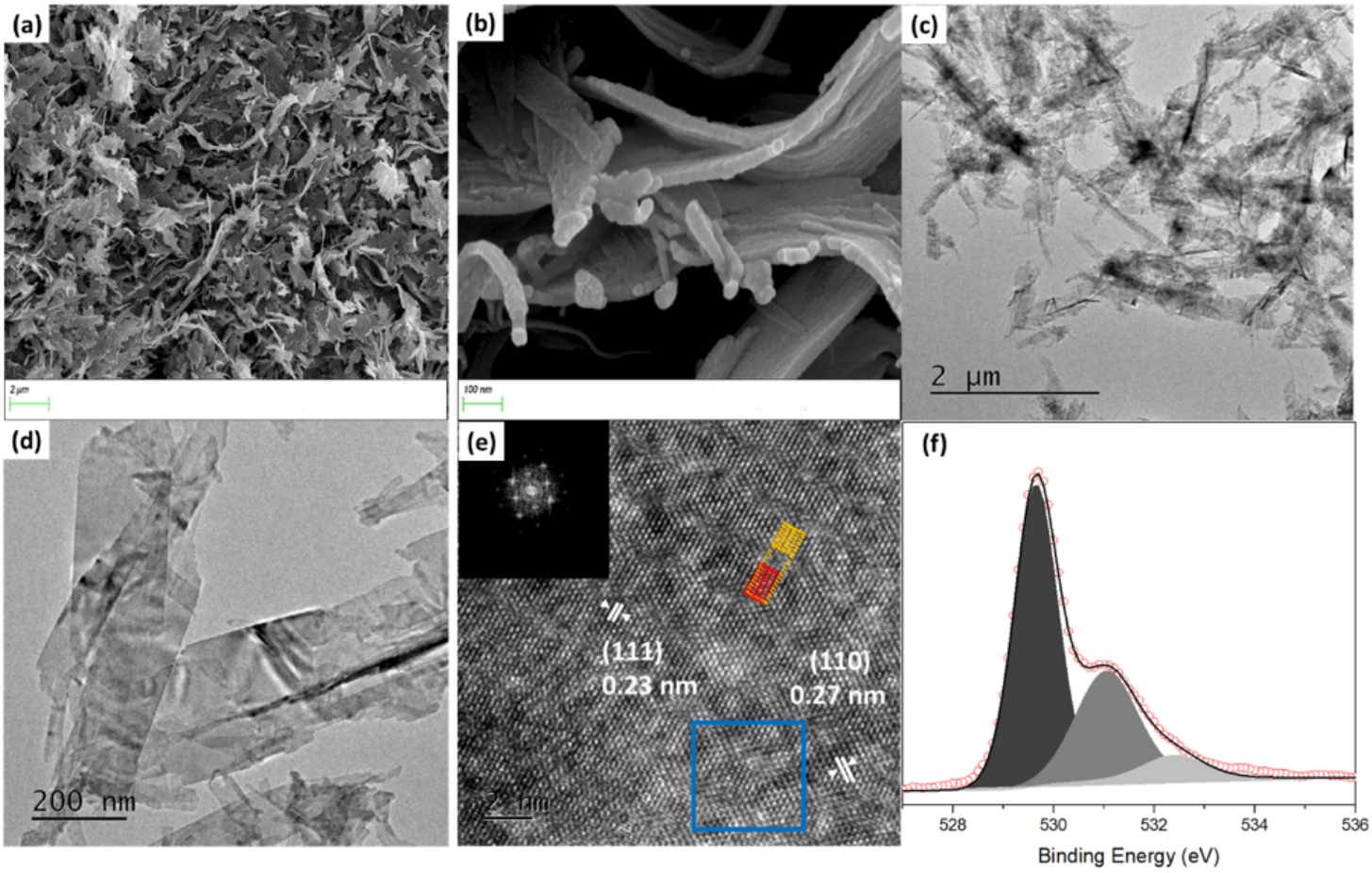

Figure 1

(a) and (b) FE-SEM images of CuO-st, (c) and (d) TEM images of CuO-st, (e) HR-TEM image of CuO-st, and (f) the XPS (O 1s region) of CuO-st.

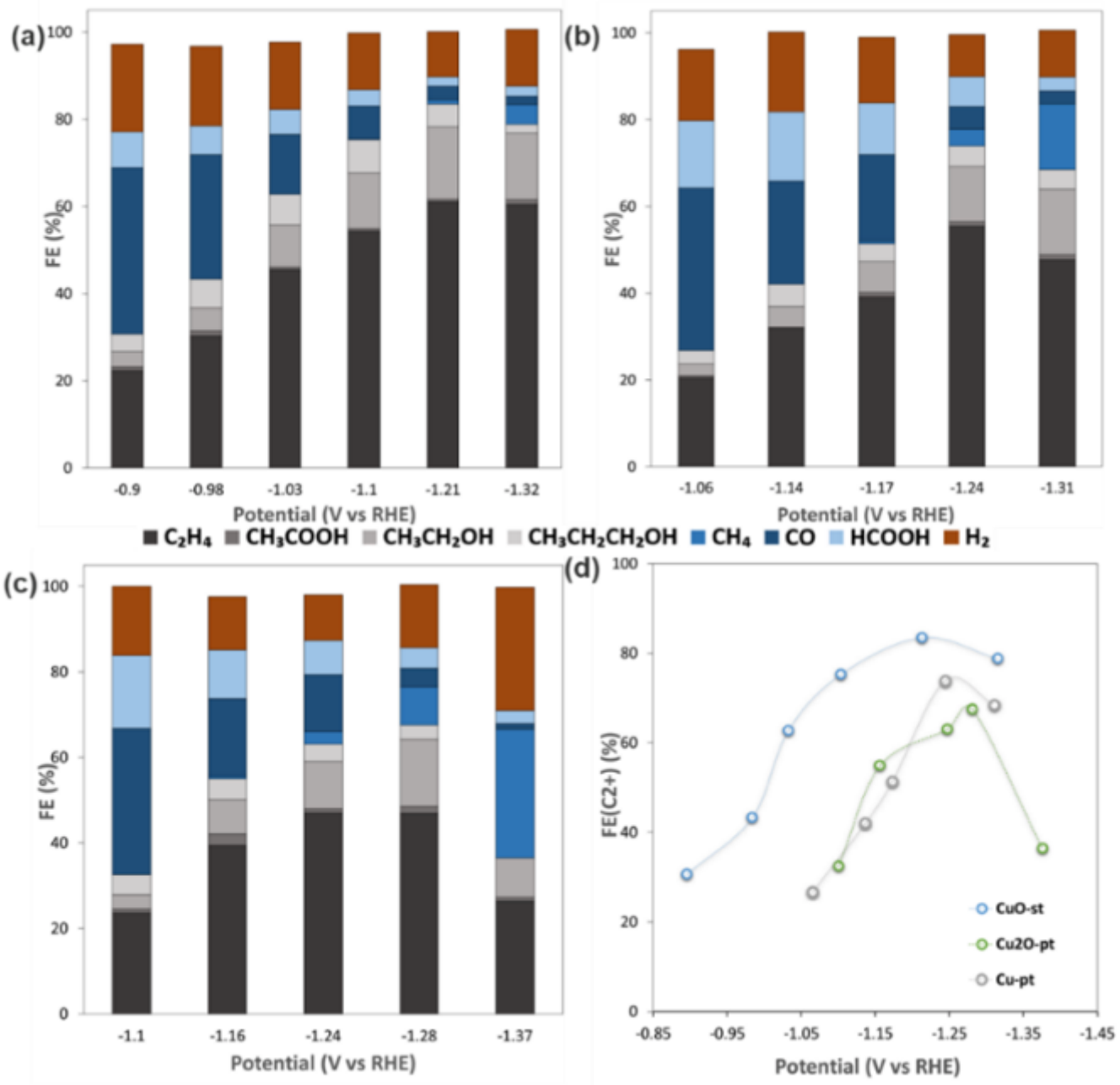

Figure 2

Product compositions vs applied potentials (with iR corrections) in 0.1M KCl on (a) CuO-st, (b) Cu2O-pt, and (c) Cu-pt; (d) the FE (C2+) of the materials

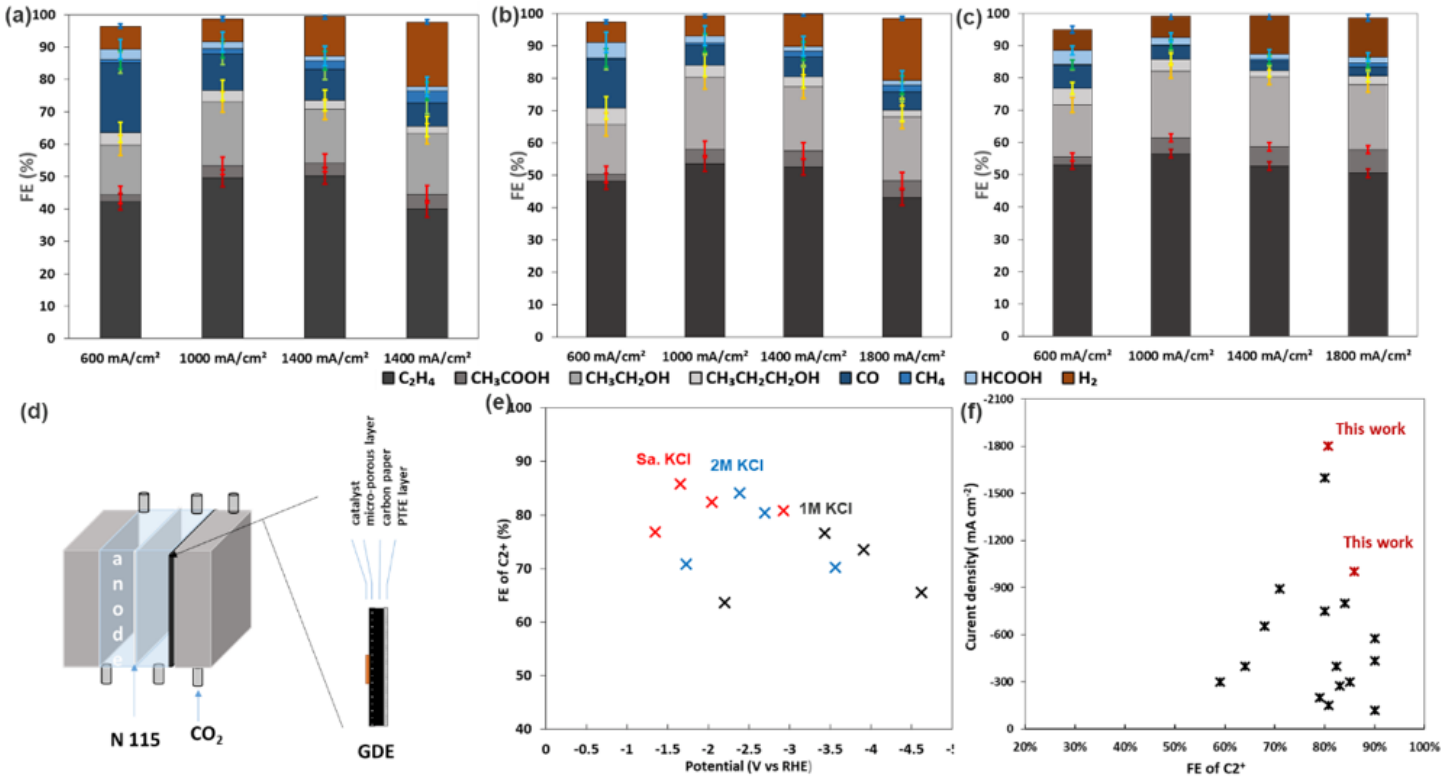

Figure 3

Product compositions vs current densities of CuO-st in (a) 1M KCl, (b) 2M KCl and (c) sa. KCl, (d) illustration of the flow cell and gas diffusion electrode (GDE), (c) FE of C2+ vs applied potentials (without iR corrections) and (d) A comparison of reported eCO2RR (see details in Supplementary Table 2)

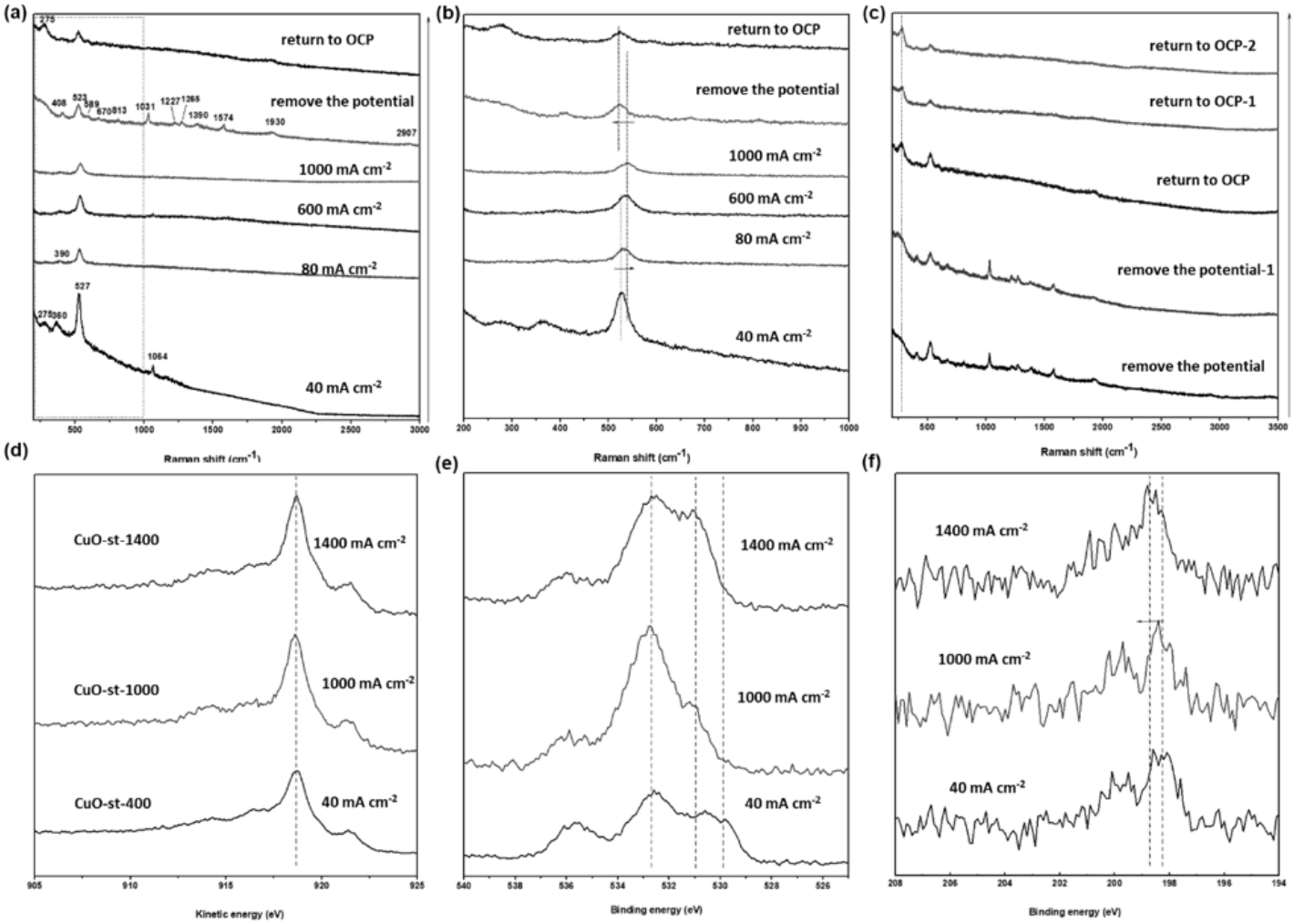

Figure 4

in situ and quasi-in situ experiments for CuO-st: (a), (b) and (c) Raman spectra, (d) the Cu LMM spectra, (e) O 1s region and (d) Cl 2p region of XPS

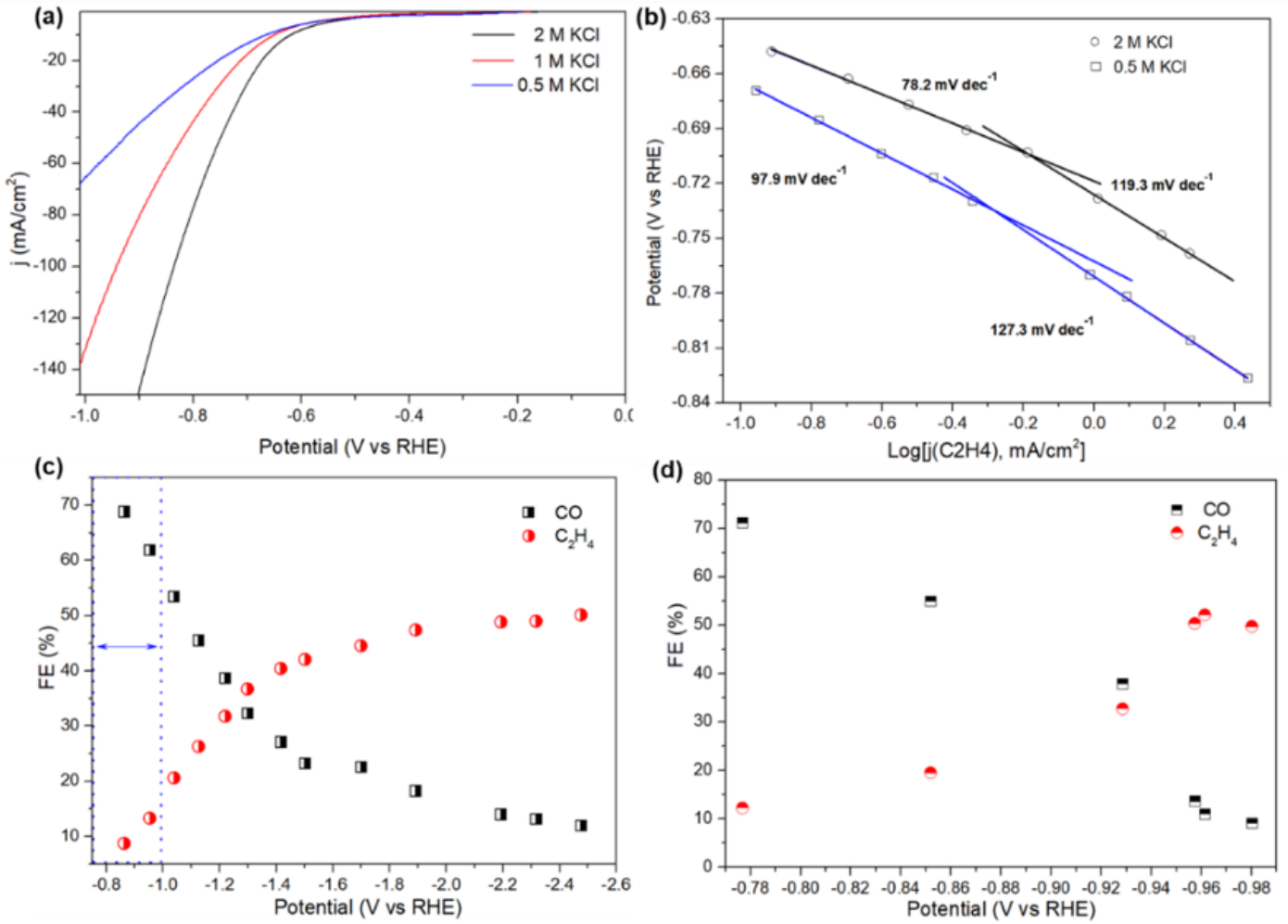

Figure 5

(a) LSV curves under CO2 atmosphere (scan rate: 50mV s-1), (b) the Tafel plots, (c) FE distribution in 0.5 M KCl, and (d) FE distribution in 2 M KCl. Note: 2 M KCl was used as the anodic electrolyte in the tests

Supplementary Files

This is a list of supplementary files associated with this preprint. Click to download.

- SupplementaryInformation.docx